10.2514/6.2015-3918

AIAA Propulsion and Energy Forum
July 27-29, 2015, Orlando, FL
51st AIAA/SAE/ASEE Joint Propulsion Conference

Advancements in the Demonstration of High Thrust to Power Ion Engine Technology

Robert E. Thomas* and Michael J. Patterson†
NASA Glenn Research Center, Cleveland, OH, 44135, USA

Jason A. Young‡ and Mark W. Crofton§
The Aerospace Corporation, El Segundo, CA, 90245, USA

John E. Foster¶
University of Michigan, Ann Arbor, MI, 48109, USA

Gridded ion thrusters provide excellent thruster performance and have successfully been implemented on both geocentric and heliocentric missions. While ion thrusters have a substantial number of attractive technological attributes, they are often classified as inherently low thrust density devices. This manuscript details an ongoing collaborative effort among the NASA Glenn Research Center, the University of Michigan, and The Aerospace Corporation investigating ion engine design modifications for high thrust-density/high thrust-to-power operation. Measurements were performed at The Aerospace Corporation in a 2.4-m diameter $\times$ 9.8-m long cryopumped vacuum chamber on an engineering model NEXT engine with a reduced interelectrode gap. The perveance, discharge losses, and far-field current density were characterized at operating conditions consistent with high thrust-to-power operation. The total voltage needed to achieve a given beam current was reduced by a factor of 10% with the reduced grid-gap optics, which is in close agreement with the Child Langmuir equation. The thrust loss correction factor ranged from 0.961 to 0.979 and was consistently higher than the predicted values. The discharge losses decreased with increasing beam current, with a minimum value of 150 W/A at a beam current of 5.50 A.

Nomenclature

A_b	= active beam area, m^2	q	= charge, C
d_s	= screen aperture diameter, m	R	= R-ratio = V_b/V_t
EM	= engineering model	TL	= throttle level
ETL	= extended throttle level	t_s	= screen electrode thickness, m
F	= thrust, N	V_a	= accelerator voltage, V
f_A	= thrust density, N/m^2	V_b	= beam voltage, V
g	= gravitational constant, m/s^2	V_d	= discharge voltage, V
I_b	= beam current, A	V_t	= total voltage = $V_b + \|V_a\|$, V
I_d	= discharge current, A	α	= ion charge thrust loss correction factor
I_{sp}	= specific impulse, s	β	= beam divergence thrust loss correction factor
j_b	= beam current density, A/m^2	δ	= current density divergence angle relative to thruster centerline
l_g	= interelectrode gap, m	ϵ_i	= discharge losses, W/A
m	= ion mass, kg	ζ	= probe angle relative to the ion optics perforated edge
NEXT	= NASA's Evolutionary Xenon Thruster	η_u	= propellant utilization efficiency
P_{in}	= input power, W	θ	= probe angle relative to ion optics centerline
PM	= prototype model	ψ	= probe angle relative to the thruster centerline at the center of the spherically-domed ion optics

*Research Engineer, In-Space Propulsion Systems Branch, 21000 Brookpark Road/MS 301-3, AIAA Member.
†Sr. Technologist, Propulsion Division, 21000 Brookpark Road/MS 301-3, AIAA Sr. Member.
‡Member of Technical Staff, Space Materials Laboratory, M2-341, P.O. Box 92957, Los Angeles, CA 90009.
§Sr. Scientist, Space Materials Laboratory, M2-341, P.O. Box 92957, Los Angeles, CA 90009, AIAA Sr. Member.
¶Associate Professor, Department of Nuclear Engineering and Radiological Sciences, 1906 Cooley Building 2355 Bonisteel Boulevard, AIAA Member

I. Introduction

Gridded ion thrusters provide excellent thruster performance and have successfully been implemented as primary propulsion on several NASA science missions.[1,2] While ion thrusters have a substantial number of attractive technological attributes, there are many perceived shortcomings of the technology. However, what are generally characterized as limitations of ion thruster technology- e.g. system complexity and low thrust density- can be more accurately characterized as attributes that have been driven by mission requirements.[3] For instance, ion thrusters are intentionally operated at low thrust densities for the purpose of achieving the extremely long lifetimes needed to support space science missions. It is possible, however, to operate these devices at thrust densities and absolute thrust levels equal to that of other high power devices that are more aligned with the requirements of earth-orbital needs.

NASA Glenn Research Center has successfully developed a number of ion propulsion systems. The NASAs Evolutionary Xenon Thruster (NEXT) project has developed next generation technologies that represent a significant advancement in technology beyond the state-of-the-art NASA Solar Technology Application Readiness thruster system. The NEXT engine incorporates a two-electrode ion optics design, has an active beam diameter of 36 cm, and nominally operates with an input power range of 0.54 - 6.9 kW. It has a maximum specific impulse of greater than 4170 seconds at a maximum thrust of greater than 236 mN, with peak efficiency in excess of 70%. During the NEXT development process, refinements to the performance and dynamic throttling range have evolved. Table 1 shows the various throttle levels for NEXT. The green entries in the table are the NEXT planetary science throttle table levels, which will be referred to as the "standard" throttle levels (TLs). These throttle levels consist of 40 discrete operating points which are defined by a unique combination of the beam current and the beam power supply voltage. These throttle levels have been extensively studied and characterized over the past decade.[4–6] Given the extraordinary lifetime capabilities of the NEXT engine established via both test[7] and analyses[8,9] for the standard throttle table, it has been determined that reducing the lifetime margin to enhance performance was a fair trade space to examine.

The yellow entries in Table 1 are the expanded throttle level (ETL) conditions, which do not require modification to the thruster or the power processor unit to implement. As such these new throttle set points could be advantageous for NASA planetary science applications, as well as earth- and cis-lunar science and commercial mission applications. The ETLs are consistent with high thrust-to-power operation, which focuses on sub- 3000 sec specific impulse operation. The gray entries correspond to high-thrust density operation, with peak thruster input power levels of 14 kW and thrust levels of 460 mN, which are conditions consistent with the electrostatic capabilities of the ion optics. A significant amount of work has been completed on characterizing the extended throttle conditions. This work includes: high thrust-to-power testing[10,11], performance and lifetime analyses[12,13], and plume characterization.[14] The blue entries in Table 1 correspond to operating conditions that were characterized during the current testing campaign, and are described in a later section.

I_b, A	V_{bps}, V												
	1800	1567	1396	1179	1021	936	850	700	679	650	400	300	275
7.04	TL56	TL55	TL54	TL53	TL52	TL51C	TL51B	TL51A					
5.80	TL51	TL50	TL49	TL48	TL47	TL46B	TL46A	TL46					
5.50	TL45G	TL45F	TL45E	TL45D	TL45C	TL45B	TL45A	TL45 (800)					
5.00	TL44G	TL44F	TL44E	TL44D	TL44C	TL44B	TL44A	TL44	TL44-660 - 540				
4.50	TL43G	TL43F	TL43E	TL43D	TL43C	TL43B	TL43A	TL43	TL43-660 - 420				
4.00	TL42G	TL42F	TL42E	TL42D	TL42C	TL42B	TL42A	TL42					
3.52	TL40	TL39	TL38	TL37	ETL3.52A	ETL3.52B	ETL3.52C	ETL3.52D	ETL3.52-660 - 360				
3.10	TL36	TL35	TL34	TL33	ETL3.1A	ETL3.1B	ETL3.1C	ETL3.1D	ETL3.1E				
2.70	TL32	TL31	TL30	TL29	TL28	ETL2.7A	ETL2.7B	ETL2.7C	ETL2.7D	ETL2.7E	TL28 (570)		
2.35	TL27	TL26	TL25	TL24	TL23	ETL2.35A	ETL2.35B	ETL2.35C	ETL2.35D	ETL2.35E			
2.00	TL22	TL21	TL20	TL19	TL18	ETL2.0A	ETL2.0B	ETL2.0C	ETL2.0D	ETL2.0E	TL18 (480)		
1.60	TL17	TL16	TL15	TL14	TL13	ETL1.6A	ETL1.6B	ETL1.6C	ETL1.6E	ETL1.6F			
1.20	TL12	TL11	TL10	TL09	TL08	TL07	TL06		TL05	TL04	TL03	TL02	
1.00													TL01

Figure 1: The NEXT ion engine throttle table (green entries), the extended throttle levels (yellow entries), the high thrust-to-power levels (gray entries), and the throttle levels of this study (blue entries).

This manuscript details an ongoing collaborative effort among the NASA Glenn Research Center, the University of Michigan, and The Aerospace Corporation investigating ion engine design modifications for high thrust-to-power operation. The next section details performance estimates and a pathway to high performance engines. Data is then presented on a NEXT engine with modified ion optics and the conclusions and future work follows.

A. Motivation

Ion engines have historically been relegated as inherently low-thrust density devices. It is instructive to investigate this claim further and define reasonable paths forward for achieving high thrust-to-power ratios. In doing so, it is useful to briefly review the pertinent analytical equations that define electrostatic engine performance. The electrostatic ion engine thrust density f_A is given by:

$$f_A = \alpha\beta\frac{I_b}{A_b}\sqrt{\frac{2mV_b}{q}} \tag{1}$$

where I_b is the beam current, V_b is the beam voltage, A_b is the beam area, and m/q is the ion mass to charge ratio. The thrust loss correction factor is the product of the doubly-charge ion thrust loss correction factor α and the plume divergence thrust loss correction factor β. The maximum beam current density is limited by the ion space charge in the gap between the screen and accelerator grids and can be expressed by a modified form of the 1-D Child-Langmuir equation, which for Xe propellant has the form:

$$j_b \approx 4.771 \times 10^{-9}\frac{V_t^{3/2}}{\left(l_g + t_s\right)^2 + \left(d_s/2\right)^2} \tag{2}$$

where V_t is the total voltage, l_g is the interelectrode gap, t_s is the screen electrode thickness, and d_s is the screen electrode aperture diameter. The current density is maximized by increasing the total voltage to the highest practical value while minimizing the ion optics geometric parameters to the lowest practical values. The specific impulse is given by:

$$I_{sp} = \alpha\beta\eta_u\frac{1}{g}\sqrt{\frac{2mV_b}{q}} \tag{3}$$

where η_u is the total propellant utilization efficiency and g is the acceleration due to gravity. To maintain a specific impulse in the sub 3000 s range, the beam voltage is held below the nominal NEXT full power value. The total voltage is held constant to maximize ion beam extraction capability, which in practice is accomplished by increasing the accelerator grid voltage V_a. This has the net effect of decreasing the R-ratio, which is defined as:

$$R \equiv \frac{V_b}{V_t} = \frac{V_b}{V_b + |V_a|} \tag{4}$$

It has been found that operating with small values of R can result in high-energy ion bombardment of the accelerator grid (potentially shortening grid life) as well as lead to an increase in the beam divergence loss.[15] The testing described in this manuscript examines the relationship between β and R-ratio. For high input power levels, P_{in} can be approximated as:

$$P_{in} \approx I_b(V_b + \epsilon_i) \tag{5}$$

Where the discharge loss ϵ_i is the discharge power divided by the beam current:

$$\epsilon_i = \frac{V_d I_d}{I_b} \tag{6}$$

The thrust-to-power ratio is for Xe propellant is then:

$$\frac{F}{P_{in}} \approx 1.650 \times 10^{-3}\alpha\beta\frac{V_b^{1/2}}{(V_b + \epsilon_i)} \tag{7}$$

It can be seen that the thrust-to-power ratio is maximized when the thrust loss parameters, beam voltage, and discharge losses are minimized. While Eqn. 2 provides an upper limit on the beam current (thrust) that can be extracted from the optics, it should be noted that state-of-the-art engines typically operate far below the Child-Langmuir limit. For instance, the maximum beam current density of the NEXT standard throttle table is only about 20% of that which can be supported by the ion optics. Figure 2 shows the maximum thrust density that is anticipated for the NEXT ion optics as predicted from the beam current density from Eqn. 2. The predicted maximum thrust density capability of the optics greatly exceeds the thrust densities associated with the standard throttle table at the total voltages of any given specific impulse.

Another design constraint that limits ion engine thrust density is the maximum supportable current. The NEXT engine utilizes a ring cusp magnetic circuit with a maximum anode current capability of 32 Amperes. At higher anode currents the discharge becomes highly resistive and unstable. In this instance the maximum thrust and thrust density are limited by the ability to produce additional ion current, and not the ability of the optics to extract additional ion current.

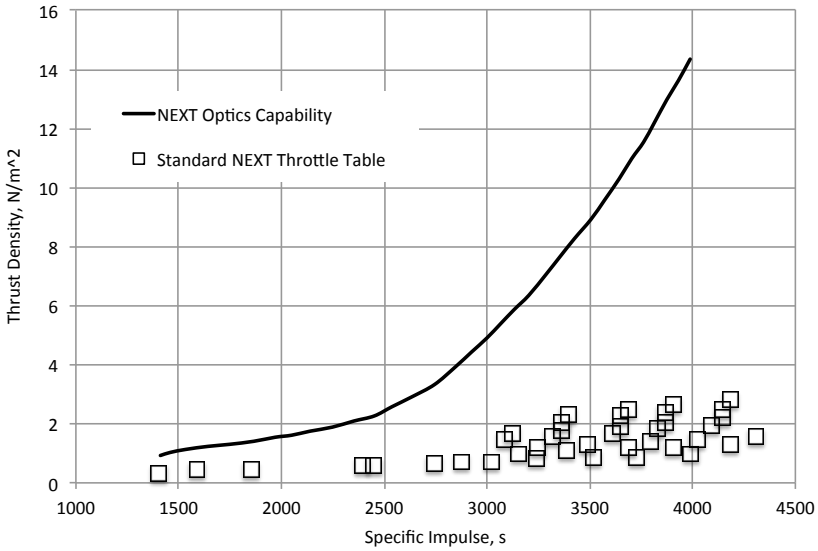

Figure 2: Comparison of NEXT performance with theorectical performance as predicted from the Child-Langmuir equation. Reproduced from Ref. [3].

This can be contrasted to the performance of a 28.7 cm beam diameter divergent field ion thruster that demonstrated a maximum anode current of 63 Amperes.[16] The innovation of the ring-cusp magnet circuit design employed in SOA thrusters has brought about significant improvements (high electrical efficiency, uniform plasma production, reduced electrode voltages and enhanced life), however the degrees of improvement must be traded against ion production. The other major constraint associated with high thrust density performance is the service lifetime of the thruster. As previously mentioned, the standard throttle levels have been thoroughly characterized, with the bulk of the 51 khr life test being run at TL 40 (3.52 A beam current), which is the harshest condition from the standpoint of accelerator grid wear. While it is clear that operating at elevated beam currents (>3.52 A) and accelerator voltages will lead to a decrease in thruster lifetime, this decrease needs to be quantified.

Reference 3 outlines the technology design paths for high-thrust density operation, which is illustrated in Fig. 3. One path (top) is the development of an annular geometry ion engine. The annular engine incorporates an annular discharge chamber, a magnetic circuit designed to circumvent ion source limiting, and high perveance flat graphite optics and is described in detail in Refs. [17–20]. The "conventional" engine pathway involves modification to a cylindical geometry such as the NEXT engine. These changes include a reduction in the interelectrode gap and/or a reduction of the screen grid thickness to increase the perveance, as well as changes in the discharge magnetic field topology. The testing described in this paper focuses on a reduction in the nominal NEXT interelectrode gap. Figure 4 shows the performance envelope for the 12.5 kW NASA Hall thruster,[21] the BPT-4000,[22] the NEXT engine, and the annular geometry ion engine. It can be seen that both ion engine technologies have demonstrated performance that encapsulates Hall thruster technologies, including operation in the sub-3000 sec specific impulse range.

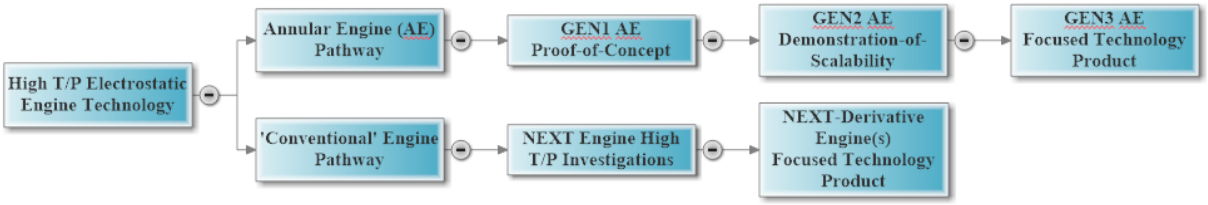

Figure 3: Development plan for high thrust density ion engines.

To summarize, there appears to be significant room for improvement in achieving high thrust density performance. The goals of the current research path with the NEXT engine are to:

1. Establish baseline performance for NEXT to go forward and modify the hardware (e.g. modify the optics to boost β, modify the discharge magnetic circuit to boost ϵ_i);
2. Ascertain the impact of grid gap change on perveance (to boost f_A), performance (F/P_{in}), and β;
3. Understand the sensitivities of β and ϵ_i as functions of high beam currents and low R-ratio.

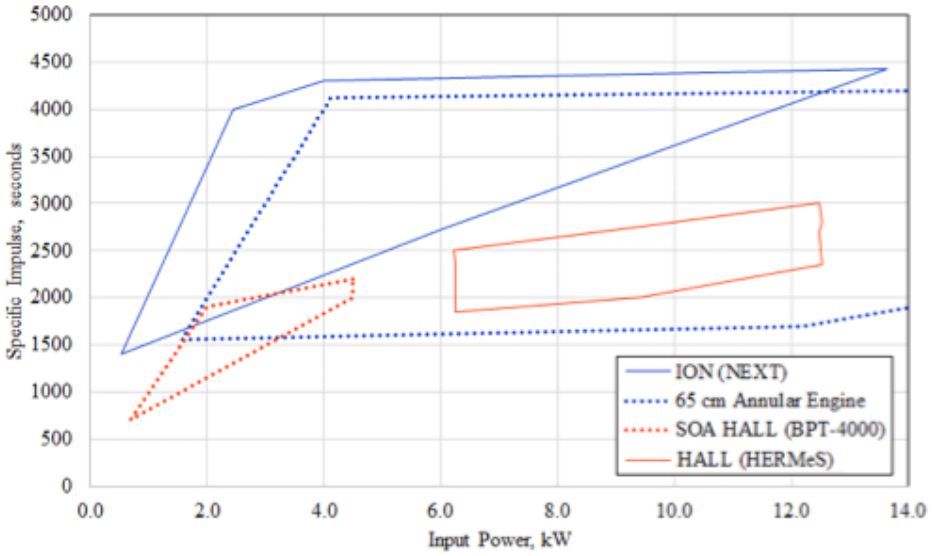

Figure 4: Comparison of electrostatic engine performance envelopes.

II. Apparatus

A. Facility

Measurements were performed at The Aerospace Corporation in a 2.4-m diameter $\times$ 9.8-m long cryopumped vacuum chamber with the thruster oriented along the chamber centerline. The base pressure with no gas load was 1×10^{-7} torr, with the residual gas being water vapor, air, and hydrocarbons. The chamber is lined with carbon composite sheets and flexible graphite to minimize the yield of sputtered material. Background pressure was measured by an ionization gauge located on the tank wall adjacent to the thruster. With an 800 V, 5.53 A beam the xenon pressure was 3.9×10^{-6} torr. The effective pumping speed for this condition was 2.9×10^{5} liter/s.

B. Test Article

Five engineering model thrusters have been manufactured at Glenn Research Center and tested. Engineering model 4 (EM-4) was used for the tests reported in this paper. The thruster utilizes a partial-conic discharge chamber, a ring-cusp magnetic circuit, and 36 cm beam diameter ion optics. The discharge cathode assembly consists of a hollow cathode with an enclosed keeper electrode fabricated of graphite, and the neutralizer cathode assembly has a high degree of NSTAR heritage. The PM thruster design includes significant enhancements over the EM thruster design including: innovative coatings to increase emissivity for enhanced thermal margin, more uniform ion optics apertures with much shallower cusps, masked ion optics to reduce edge-hole erosion, and graphite discharge cathode keeper to mitigate keeper erosion.[6] Detailed descriptions of the EM and PM designs can be found in Refs. 23 and 24, respectively. The thruster was operated using commercially available power supplies and integrated recycle logic circuitry, allowing for thruster input powers up to 10 kW with beam power supply voltages up to 2000 V. A calibrated, high-purity xenon feed system was used to deliver xenon propellant to the discharge cathode, neutralizer cathode, and discharge chamber main plenum through individual mass flow controllers.

C. Plasma Diagnostics

Measurements of the beam current density were made 273 cm from the accelerator electrode to determine beam divergence. The beam current density was measured with a conventional guard-ring planar probe using the rotating arm to scan in a grid-normal orientation at a constant distance (Fig. 5). The collector diameter was 1.27 cm and the guard ring outer diameter was 2.54 cm. For the far-field scans the thruster was pivoted 12°away from chamber centerline to expand the angular range, and the probe axis of rotation coincided with the center of curvature of the spherically-domed ion optics.

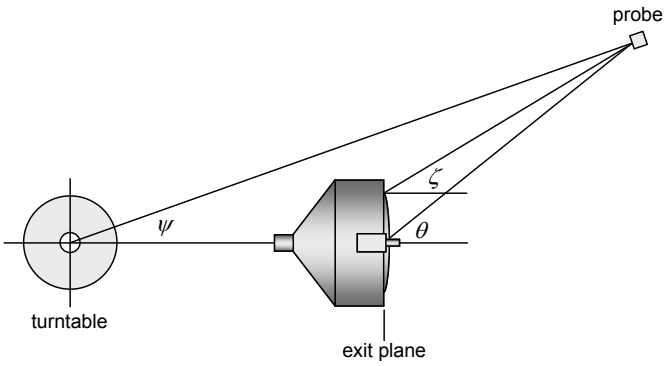

Figure 5: Schematic of plasma diagnostics for far-field current density measurements.

III. Experimental Results

Data were collected at the 26 operating conditions shown in Table 1. This included, in part, five conditions from the standard throttle table, and four throttle levels that were modified ("MOD") by decreasing the beam voltage from the nominal value in order to increase the thrust density. Extended data sets were collected at beam currents of 3.52, 4.50, and 5.00 A. This was done to understand the influence of the R-ratio on β; this was accomplished by fixing the beam current and simultaneously decreasing V_b and increasing the V_a. The peak thrust-to-power ratio occurs at ETL3.52-360; at this condition: $F/P_{in} = 54$ mN and the specific impulse is 1826 seconds.

Table 1: Operating conditions for high thrust-to-power testing.

TL	J_b, A	V_{bps}, V	V_a, V	V_t, V	R-ratio	F/P, mN/kW	I_{sp}, s
3	1.20	400	-310	710	0.548	44	1855
3MOD	1.20	400	-200	600	0.648	44	1861
5	1.20	679	-115	794	0.841	42	2447
18	2.00	1021	-175	1196	0.844	41	3237
18MOD	2.00	480	-175	655	0.715	49	2194
28	2.70	1021	-175	1196	0.844	42	3117
28MOD	2.70	570	-175	745	0.749	49	2321
37	3.52	1179	-200	1379	0.846	41	3386
37MOD	3.52	660	-200	860	0.754	48	2504
ETL 3.52-360	3.52	360	-500	860	0.405	54	1826
ETL 3.52-420	3.52	420	-440	860	0.475	53	1986
ETL 3.52-480	3.52	480	-380	860	0.545	52	2131
ETL 3.52-540	3.52	540	-320	860	0.614	51	2269
ETL 3.52-600	3.52	600	-260	860	0.684	49	2407
ETL 3.52-660	3.52	660	-200	860	0.754	48	2531
43	4.50	700	-400	1100	0.625	48	2633
43-420	4.50	420	-560	980	0.416	53	2010
43-480	4.50	480	-520	1000	0.468	52	2158
43-540	4.50	540	-480	1020	0.518	51	2298
43-600	4.50	600	-440	1040	0.565	50	2432
43-660	4.50	660	-400	1060	0.611	49	2555
44	5.00	700	-500	1200	0.572	48	2671
44-540	5.00	540	-580	1120	0.471	51	2336
44-600	5.00	600	-540	1140	0.515	50	2471
44-660	5.00	660	-500	1160	0.559	49	2587
45-800	5.53	800	-540	1340	0.588	46	2873

The discharge losses as a function of the beam current is shown in Fig. 6. As the beam current is increased the xenon ionization rate also increases; it has been shown that this leads to a decrease in the discharge losses.[25] From Eqn. 7 the decrease in discharge losses as the beam current is increased is beneficial from the standpoint of optimizing the thrust-to-power ratio.

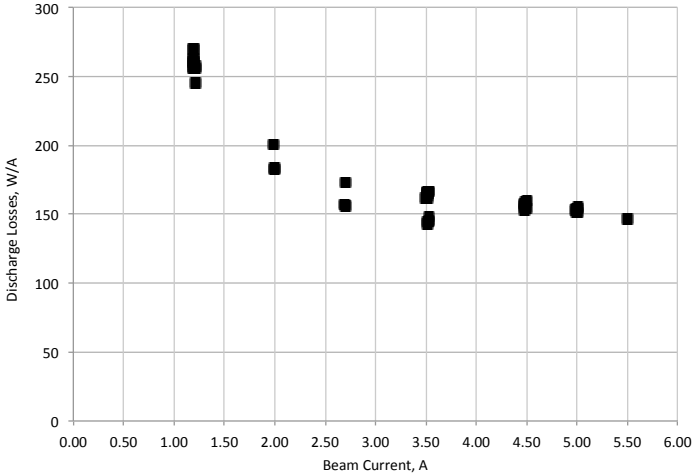

Figure 6: Discharge losses vs. beam current.

The impingement-limited total voltage is a measure of the current extraction capability of the ion optics and is determined from plots of accelerator current as a function of total voltage (Fig. 7). The perveance limited voltage is defined as the voltage where the slope is -0.02 mA/V. The measured perveance for both nominal and re-gapped electrodes is shown in Fig. 8. For a fixed beam current, the total voltage was expected to decrease according to Eqn. 8, which predicts that reducing the grid gap by 21% will lead to an 11% decrease in the total voltage. It should be noted that the grip gap is not constant along the span of the electrodes; an average cold gap value was used for the calculations. It can be seen that the simplified 1-D Child Langmuir equation provides a reasonable estimate of the total voltage, and is within 5% of the experimental values.

$$\frac{V_{t,re-gap}}{V_{t,nom}} = \left[\frac{\left(l_{g,re-gap} + t_s\right)^2 + \left(d_s/2\right)^2}{\left(l_{g,nom} + t_s\right)^2 + \left(d_s/2\right)^2}\right]^{2/3} \tag{8}$$

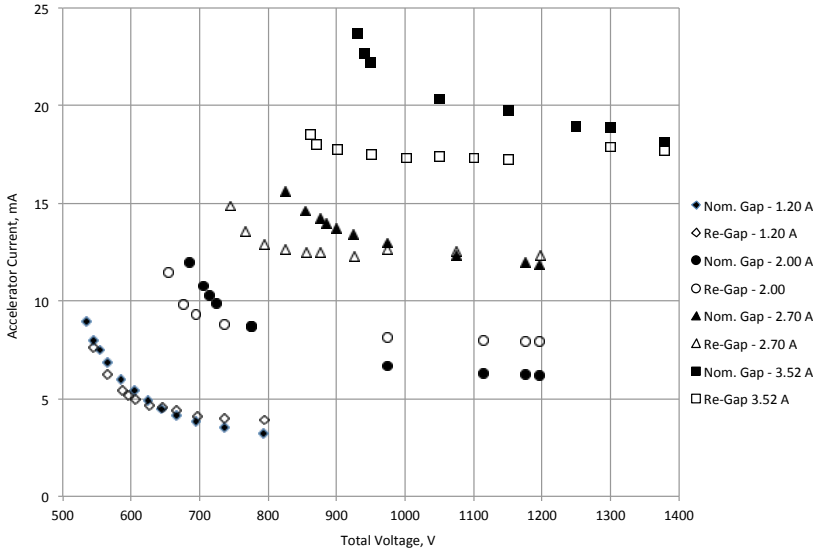

Figure 7: Accelerator current vs. total voltage.

Representative current density traces as measured by the planar probe are shown in Fig. 9. The beam divergence thrust-loss factor is experimentally found using the methodology described by Pollard in Ref. 26, and is calculated using Eqn. 9. The integrand in the numerator is the product of the axial component of beam current density $j_b \cos(\delta)$ and the area weighting factor $\sin(\psi)\ \mathrm{d}\psi$. The scan range was from ψ = 0°to 29.5°in 0.5°steps, i.e. δ = 0°to -33.0°. For integrating Eqn. (9), the data are extrapolated to reduce the truncation error by assuming an exponential fall-off in j_b vs. ψ for angles between 29.5°and 45°(Fig. 9).

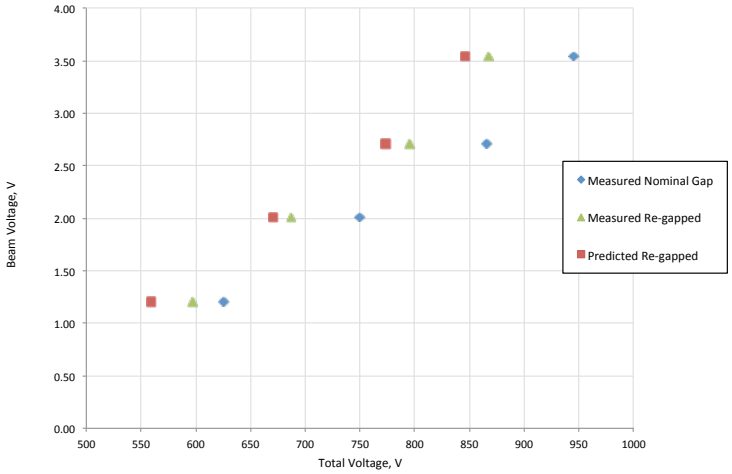

Figure 8: Beam current vs. total voltage for reduced grid gap optics.

$$\beta = \frac{\int_0^{-45^\circ} j_b \cos(\delta) \sin(\psi)\, \mathrm{d}\psi}{\int_0^{-45^\circ} j_b \sin(\psi)\, \mathrm{d}\psi} \tag{9}$$

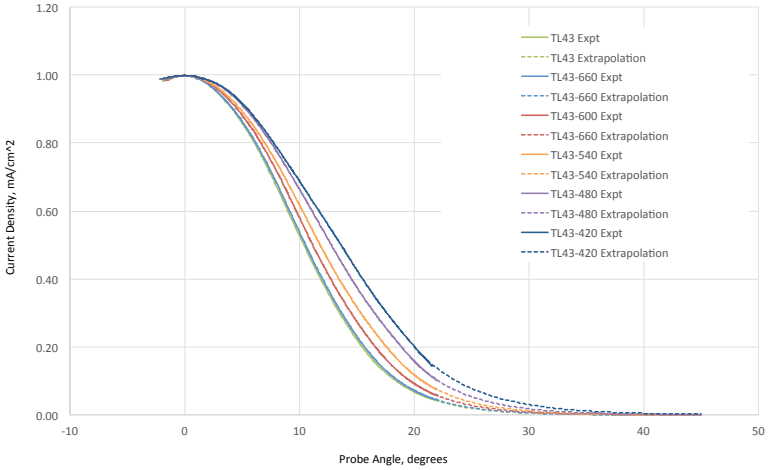

Figure 9: Beam current density vs. probe angle for the re-gapped EM-4 engine.

The thrust loss divergence factors calculated from the current density measurements are shown in Fig. 10 for nineteen different operating conditions. As expected, the beam divergence increases with decreasing R-ratio, which is consistent with prior ion optic studies.[27] An empirical equation for calculating β was obtianed from a curve fit of experimental data in Ref. [10]:

$$\beta_{fit} = \beta^* - 0.1470 + 0.8440(R) - 20.675(R)^2 + 2.3661(R)^3 - 1.0167(R)^4 \tag{10}$$

The β^* term is a normalization constant that takes into account the: 1) accelerator-to- screen grid aperture diameter ratio; 2) accelerator grid thickness-to-screen grid aperture diameter ratio, and 3) the grid gap-to-screen grid aperture diameter ratio. It can be seen from Fig. 10 that the predicted β accurately captures the trends in beam divergence, and is generally in close agreement to the experimental values. The divergence data for throttle levels 5 and 37 are compared to the PM1R data that Pollard collected in Table 2. The EM-4 β value is within the error bar measurement at the PM1R measurement at TL 5, and is 1% less than the PM1R value at TL37, which illustrates that re-gapping the optics did not lead to a significant increase in the beam divergence for a given operating condition. The measured

values are consistent with projected performance of the thruster, and Eqn. 10 provides a reasonable estimate for the operating conditions tested, and will continue to be used for future estimations of performance.

Table 2: Comparison of experimental β values for EM-4 and PM1R.

TL	β (PM1R)	β (Re-gapped EM-4)
5	0.977	0.972
37	0.974	0.965

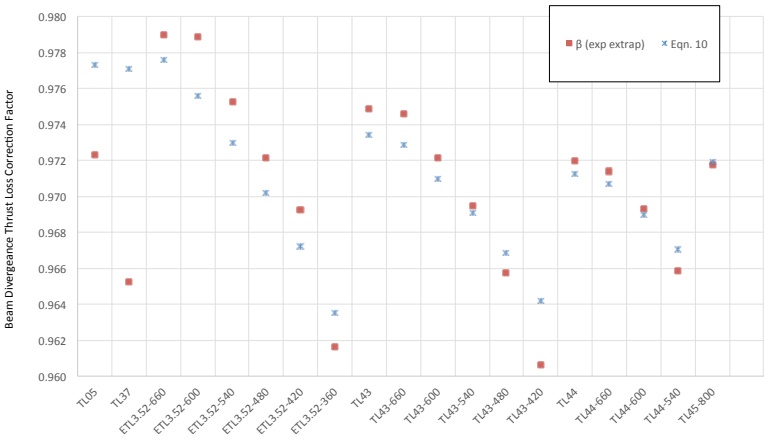

Figure 10: Divergence Loss Correction Factor for re-gapped EM-4 Engine.

IV. Summary & Future Work

Measurements were performed on an engineering model NEXT engine with a modified ion optics geometry in order to investigate the influence of electrode gap on beam divergence and discharge losses. The perveance, discharge losses, and far-field ion density were characterized at operating conditions consistent with high-thrust-to-power ratio operation at beam currents in the range of 1.20-5.53 A. The total voltage needed to achieve a fixed beam current was reduced by a factor of 10% with the reduced grid-gap optics, which is in close agreement with the 1-D Child Langmuir equation. The thrust loss correction factor, as measured using a planar Faraday probe, ranged from 0.961 to 0.979 and was modelled accurately using a previously developed polynomial fit. The discharge losses decreased with increasing beam current, with a minimum value of 150 W/A at a beam current of 5.50 A.

Two paths have been discussed that will provided near term opportunities for high thrust density and high thrust-to-power ion engine operation: 1) modifying conventional cylindrical geometry ion engines by incorporating advanced design ion optics and/or divergent field magnetic field topologies; and the 2) development of annular ion engine geometries. The latter route is further discussed in a companion paper. The results presented in this paper are the first step in the investigation of high thrust density operation by making straight-forward alterations to the NEXT engine. The preliminary results are encouraging, and it should be noted that the test was not limited the capability of the ion optics, but by the discharge and accelerator power supply that were used for the test. A 20 kW power console with higher output discharge and accelerator capabilities has been assembled and will be used for future tests.

Acknowledgments

The authors acknowledge Mr. Kevin McCormick of NASA Glenn Research Center for work on thruster design, fabrication, and assembly. This work was supported under the Glenn Research Center Center Innovation Fund program sponsored by NASA's Office of Chief Technologist, and The Aerospace Corporation's Independent Research and Development Plan.

References

[1]Polk, J., Kakuda, R., Anderson, J., and Brophy, J., "Performance of the NSTAR Ion Propulsion System on the Deep Space One Mission," *39^{th} AIAA Aerospace Sciences Meeting & Exhibit*, Reno, NV, Jan. 8-11 2001, AIAA-2001-0965.

[2]Brophy, J., Garner, C., Nakazono, B., Marcucci, M., Henry, M., and Noon, D., "The Ion Propulsion System for Dawn," *39^{th} AIAA/ASME/SAE/ASEE Joint Propulsion Conference and Exhibit*, Huntsville, AL, July 20-23, 2003, AIAA-2003-4542.

[3]Patterson, M. J., "Development Status of High-Thrust Density Electrostatic Engines," *50^{th} AIAA/ASME/SAE/ASEE Joint Propulsion Conference and Exhibit*, Cleveland, OH, July 28-30, 2014, AIAA-2014-3422.

[4]Soulas, G. C., Domonkos, M. T., and Patterson, M. J., "Performance Evaluation of the NEXT Ion Engine," *39^{th} AIAA/ASME/SAE/ASEE Joint Propulsion Conference and Exhibit*, Huntsville, AL, July 20-23, 2003, AIAA-2003-5278.

[5]Soulas, G. C. and Patterson, M. J., "NEXT Ion Thruster Performance Dispersion Analyses," *43^{rd} AIAA/ASME/SAE/ASEE Joint Propulsion Conference and Exhibit*, Cincinnati, OH, July 8-11, 2007, AIAA-2007-5213.

[6]Herman, D. A., Soulas, G. C., and Patterson, M. J., "Performance Evaluation of the Prototype-Model NEXT Ion Thruster," *43^{rd} AIAA/ASME/SAE/ASEE Joint Propulsion Conference and Exhibit*, Cincinnati, OH, July 8-11, 2007, AIAA-2007-5213.

[7]Shastry, R., Herman, D. A., Soulas, G. C., , and Patterson, M. J., "End-of-Test Performance and Wear Characterization of NASAs Evolutionary Xenon Thruster (NEXT) Long-Duration Test," *50^{th} AIAA/ASME/SAE/ASEE Joint Propulsion Conference and Exhibit*, Cleveland, OH, July 28-30, 2014, AIAA-2014-3617.

[8]Van Noord, J., "Lifetime Assessment of the NEXT Ion Thruster," *43^{rd} AIAA/ASME/SAE/ASEE Joint Propulsion Conference and Exhibit*, Cincinnati, OH, July 8-11, 2007, AIAA-2007-5274.

[9]Van Noord, J. and Herman, D. A., "Lifetime Assessment of the NEXT Ion Thruster," *44^{th} AIAA/ASME/SAE/ASEE Joint Propulsion Conference and Exhibit*, Hartford, CT, July 21-23, 2008, AIAA-2008-4526.

[10]Patterson, M. J., "NEXT Study of Thruster Extended Performance (NEXT STEP)," *42^{nd} AIAA/ASME/SAE/ASEE Joint Propulsion Conference and Exhibit*, Sacramento, CA, July 9-12, 2006, AIAA-2006-4664.

[11]Patterson, M. J., Soulas, G. C., Young, J. A., and Crofton, M. W., "Expanded Throttling Capabilities of the NEXT Thruster," *49^{th} AIAA/ASME/SAE/ASEE Joint Propulsion Conference and Exhibit*, San Jose, CA, July 14-17, 2013, AIAA-2013-3891.

[12]Patterson, M. J., "NEXT Study of Thruster Extended Performance II (NEXT STEP II)," *44^{th} AIAA/ASME/SAE/ASEE Joint Propulsion Conference and Exhibit*, Hartford, CT, July 21-23, 2008, AIAA-2008-4808.

[13]Patterson, M. J., Pinero, L., and Sovey, J. S., "Near-Term High Power Ion Propulsion Options for Earth-Orbital Applications," *45^{th} AIAA/ASME/SAE/ASEE Joint Propulsion Conference and Exhibit*, Denver, CO, August 2-5, 2009, AIAA-2009-4819.

[14]Young, J. A., Crofton, M. W., Diamant, K. D., and Patterson, M. J., "Plume Characterization of the NEXT Thruster Under Extended Throttle Conditions," *49^{th} AIAA/ASME/SAE/ASEE Joint Propulsion Conference and Exhibit*, San Jose, CA, July 14-17, 2013, AIAA-2013-4111.

[15]Aston, G. and Kaufman, H., "The Ion-Optics of a Two-Grid Electron-Bombardment Thruster," *AIAA International Electric Propulsion Conference*, Key Biscayne, FL, November 14 - 17, 1976, AIAA-P–76-1029.

[16]Patterson, M. J. and Rawlin, V. K., "Performance of 10 kW Class Xenon Ion Thrusters," *24^{th} AIAA/ASME/SAE/ASEE Joint Propulsion Conference and Exhibit*, Boston, MA, July 11-13, 1988, AIAA-1988-2914.

[17]Patterson, M. J., "Next Generation Electric Propulsion Thrusters," *47^{th} AIAA/ASME/SAE/ASEE Joint Propulsion Conference and Exhibit*, San Diego, CA, July 31 - August 3, 2011, AIAA-2011-5812.

[18]Patterson, M. J., Herman, D. A., Shastry, R., and Van Noord, J., "Annular-Geometry Ion Engine: Concept, Development Status, and Preliminary Performance," *48^{th} AIAA/ASME/SAE/ASEE Joint Propulsion Conference and Exhibit*, Atlanta, GA, July 30 - August 1, 2012, AIAA-2012-3798.

[19]Shastry, R., Patterson, M. J., Herman, D. A., and Foster, J. E., "Current Density Measurements of an Annular Geometry Ion Engine," *48^{th} AIAA/ASME/SAE/ASEE Joint Propulsion Conference and Exhibit*, Atlanta, GA, July 30 - August 1, 2012, AIAA-2012-4186.

[20]Patterson, M. J., Foster, J. E., Young, J. A., and Crofton, M. W., "Annular Engine Development Status," *49^{th} AIAA/ASME/SAE/ASEE Joint Propulsion Conference and Exhibit*, San Jose, CA, July 14-17, 2013, AIAA-2013-3892.

[21]Kamhawi, H., Huang, W., Haag, T., Yim, J., Chang, L., Clayman, L., Herman, D. A., Shastry, R., Thomas, R., Griffith, C., Myers, J., Williams, G., Mikellides, I. G., Hofer, R. R., Polk, J. E., and Goebel, D., "Overview of the Development of the Solar Electric Propulsion Technology Demonstration Mission 12.5-kW Hall Thruster," *50^{th} AIAA/ASME/SAE/ASEE Joint Propulsion Conference and Exhibit*, Cleveland, OH, July 28 - 30, 2014, AIAA-2014-3898.

[22]Welander, B., Carpenter, C., de Grys, K., Hofer, R. R., and Randolph, T. M., "Life and Operating Range Extension of the BPT-4000 Qualification Model Hall Thruster," *42^{nd} AIAA/ASME/SAE/ASEE Joint Propulsion Conference and Exhibit*, Sacramento, CA, July 9 - 12, 2006, AIAA-2006-5263.

[23]Patterson, M. J., Foster, J. E., Haag, T. W., Rawlin, V. K., Soulas, G. C., and Roman, R. F., "NEXT: NASA's Evolutionary Xenon Thruster," *38^{th} AIAA/ASME/SAE/ASEE Joint Propulsion Conference and Exhibit*, Indianapolis, IN, July 7 - 10, 2002, AIAA-2002-3832.

[24]Hoskins, W. A., Wilson, F. C., Polaha, J., Talerico, L., Patterson, M. J., Soulas, G. C., and Sovey, J., "Development of a Prototype Model Ion Thruster for the NEXT System," *40^{th} AIAA/ASME/SAE/ASEE Joint Propulsion Conference and Exhibit*, Fort Lauderdale, FL, July 11 - 14, 2004, AIAA-2004-4111.

[25]Goebel, D. M., Wirz, R. E., and Katz, I., "Analytical Ion Thruster Discharge Performance Model," *Journal of Propulsion and Power*, Vol. 23, No. 5, 2007, pp. 1055–1067.

[26]Pollard, J. E., Diamant, K. D., Crofton, M. W., Patterson, M. J., and Soulas, G. C., "Spatially Resolved Beam Current and Charge-State Distributions for the NEXT Ion Engine," *46^{th} AIAA/ASME/SAE/ASEE Joint Propulsion Conference and Exhibit*, Nashville, TN, July 25 - 28, 2010, AIAA-2010-6779.

[27]Aston, G., Kaufman, H., and Wilbur, P., "Ion Beam Divergence Characteristics of Two-Grid Accelerator Systems," *AIAA Journal*, Vol. 16, No. 5, 1978, pp. 516–524.